Polymer Journal (2018) 50:889–898
https://doi.org/10.1038/s41428-018-0051-9

ORIGINAL ARTICLE

Liquid-crystalline behavior and ion transport properties of block-structured molecules containing a perfluorinated ethylene oxide moiety complexed with a lithium salt

Taira Onuma[1] · Masafumi Yoshio[1,3] · Masaki Obi[2] · Kimiaki Kashiwagi[2] · Shinya Tahara[2] · Takashi Kato[1]

Received: 25 January 2018 / Revised: 8 March 2018 / Accepted: 8 March 2018 / Published online: 18 April 2018
© The Society of Polymer Science, Japan 2018

Abstract

The liquid-crystalline behavior of fluorinated block-structured molecules and the ion transport properties of their complexes with a Li salt have been examined. The block-structured molecules comprise a perfluorinated oligo (ethylene oxide) moiety containing a terminal methyl carbonate or a terminal hydroxyl group and an octadecyl moiety. These molecules exhibit highly ordered smectic phases. The fluorinated molecule with a terminal methyl carbonate possesses an isotropization temperature lower than that of the analogous non-fluorinated molecule. The fluorinated molecule complexed with a Li salt shows ionic conductivities on the order of 10^{-6} S cm^{-1} in the smectic phase formed at ambient temperature, while conductivities on the order of 10^{-5} S cm^{-1} are observed in the isotropic phase.

Introduction

Nanostructured liquid crystals have attracted attention for applications in the transport of ions [1–8], electrons [9–13], and molecules [14–18] owing to the anisotropic properties of these materials. The transport of ions in 1D [19, 20], 2D [21–24], and 3D [25–29] nanochannels of columnar, smectic, and bicontinuous cubic structures has been achieved for these nanostructured liquid-crystalline (LC) materials. Among these properties, 2D transport in layered nanostructured liquid crystals has been applied to Li-ion batteries (LIBs) [30, 31]. A cyclic carbonate-based LC electrolyte with layered ionic pathways showed a relatively high ionic conductivity and electrochemical stability suitable for operation in LIBs, resulting in reversible charge-discharge processes for both the positive and negative electrodes [30]. Other LC electrolytes containing poly- or oligo (ethylene oxide) [21, 23], imidazolium [20, 23], ammonium [25], phosphonium [25], and zwitterionic [24, 26, 27] moieties have also been developed for potential application in LIBs.

In general, the mechanism of Li ion conduction in poly (ethylene oxide) (PEO) occurs as follows [32–34]: ether oxygens coordinate to Li cations, leading to the dissociation of Li salts. The dissociated Li cations can be transported through segmental motion of the polymer chains. The coordination structures of the ether oxygens with Li cations is relatively stable. Because of these polymer-coordinated structures of Li cations, the diffusion of the cations is usually slower than that of the anions. In contrast, the coordination of the ether oxygens contained in a perfluorinated oligoether to metal ions is weaker than the coordination of those in a non-fluorinated oligoether; perfluorinated ethers do not coordinate metal ions at all [35]. This difference is due to the weaker Lewis basicity of the ether oxygens resulting from the inductive electron-withdrawing effect of the fluoro substituents. Instead, these compounds preferentially coordinate anions over cations [36].

✉ Takashi Kato
kato@chiral.t.u-tokyo.ac.jp

[1] Department of Chemistry and Biotechnology, School of Engineering, The University of Tokyo, Hongo, Bunkyo-ku, Tokyo 113-8656, Japan

[2] Asahi Glass Co. Ltd., Research Center, Hazawa-cho, Kanagawa-ku, Yokohama, Kanagawa 221-8755, Japan

[3] Present address: Semiconductor Nano-interfaces Group, Research Center for Functional Materials, National Institute for Materials Science, Namiki, Tsukuba, Ibaraki 305-0044, Japan

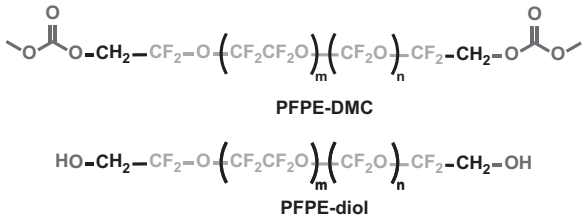

Fig. 1 Molecular structures of PFPE-based electrolytes reported by Wong et al [37–40].

Recently, the application of perfluoropolyether (PFPE)-based electrolytes in LIBs was proposed by DeSimone and Balsara et al [37–43]. The researchers developed low-molecular-weight PFPEs complexed with lithium bis(trifluoromethylsulfonyl)imide (LiTFSI) (Fig. 1). The electrochemical performance of these electrolytes in Li batteries was evaluated through cycling tests of a cell composed of Li metal and $LiNi_{1/3}Co_{1/3}Mn_{1/3}O_2$ as the anode and cathode, respectively, and the electrolytes exhibited potential for application in LIBs. LIBs with these electrolytes are expected to show enhanced safety and durability because of their nonflammability, thermal stability, and electrochemical stability. These electrolytes also showed an excellent lithium transference number close to unity (>0.9). The researchers explained that this ion-conducting behavior results from (1) solvation of the perfluorinated anions in the PFPEs and (2) weakened coordination of the carbonyl groups to Li cations caused by the fluoro substituents in the polymers. The researchers also developed hybrid electrolytes with inorganic sulfide glass particles that exhibited single ion-conducting behavior and limited the dissolution of lithium polysulfides. Thus, these electrolytes are potentially applicable to lithium-sulfur batteries [38].

The self-assembly of nanosegregated structures is often driven by molecules having perfluorinated moieties through the immiscible nature of the perfluorinated and non-fluorinated parts [44–47]. For example, block-structured semifluorinated alkanes exhibit LC properties that originate from the immiscibility of the block segments and the rigidity of the fluorocarbons [48–53]. We previously developed LC Li ion conductors bearing perfluoroalkyl chains at the termini of the mesogenic parts [54]. The introduction of a perfluorinated moiety resulted in an improvement in the thermal stability of the LC phases, which led to enhanced ionic conductivities in a wider temperature range compared to those of the analogous non-fluorinated molecules. We expected that the nanosegregation of the immiscible perfluorinated sections and hydrocarbon groups can drive the formation of LC structures. Our intention here is to examine the effects of a perfluorinated oligo (ethylene oxide) moiety on the LC properties and ionic conductivity.

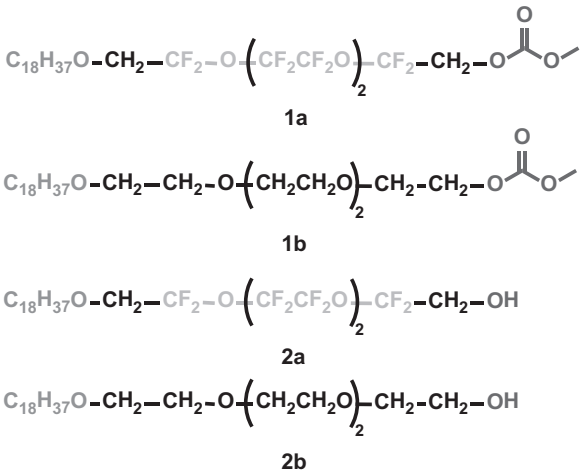

Fig. 2 Molecular structures of fluorinated block-structured molecules and analogous non-fluorinated molecules with a terminal methyl carbonate (**1a** and **1b**) or a terminal hydroxyl (**2a** and **2b**) group

In the present study, fluorinated block-structured molecules containing a perfluorinated oligo (ethylene oxide) moiety and an alkyl group (**1a** and **2a**) have been developed (Fig. 2). For comparison, non-fluorinated molecules (**1b** and **2b**) have also been prepared, and their properties have been examined.

Experimental procedures

General procedures

NMR spectra were recorded on a JEOL JNM-ECX400 instrument at 400 MHz for ^{1}H NMR spectroscopy, 100 MHz for ^{13}C NMR spectroscopy, and 376 MHz for ^{19}F NMR spectroscopy. The chemical shifts of the ^{1}H, ^{13}C, and ^{19}F NMR signals were referenced to the Me_4Si internal standard ($\delta = 0.00$), residual $CDCl_3$ ($\delta = 77.16$), and C_6F_6 ($\delta = -164.90$), respectively, and described in terms of the chemical shift in ppm (δ), multiplicity, coupling constant (Hz), and relative intensity. Matrix-assisted laser desorption ionization time-of-flight mass spectra (MALDI-TOF MS) were obtained using a Bruker Daltonics Autoflex Speed instrument using *trans*-2-[3-(4-*tert*-butylphenyl)-2-methyl-2-propenylidene] malononitrile as the matrix. The thermal properties of the materials were examined by differential scanning calorimetry (DSC) using a Netzsch DSC204 Phoenix system. The heating and cooling rates were both 10 K min^{-1}. The transition temperatures were taken at the onsets of the transition peaks on first cooling. An Olympus BX53 polarizing optical microscope (POM) equipped with a Linkam LTS350 hot stage was used to study the LC properties. X-ray diffraction (XRD) patterns were taken on

a Rigaku RINT-2500 diffractometer with CuKα radiation. Molecular mechanics calculations were carried out by the Gaussian 09 W software package.

Materials

2,2,4,4,5,5,7,7,8,8,10,10-Dodecafluoro-3,6,9-trioxaundecane-1, 11-diol was supplied by Asahi Glass Co. Ltd., and all other reagents and solvents used for the synthesis were purchased from commercially available sources and used as received without further purification.

Synthesis of 2,2,4,4,5,5,7,7,8,8,10,10-dodecafluoro-3,6,9,12-tetraoxatriacontan-1-ol (2a)

1-Bromooctadecane (726 mg, 2.18 mmol), 2,2,4,4,5,5,7,7,8, 8,10,10-Dodecafluoro-3,6,9-trioxaundecane-1,11-diol (2.052 g, 5.00 mmol), and K_2CO_3 (440 mg, 3.18 mmol) in DMF (15 mL) were stirred at 80 °C for 2 h. A saturated aqueous NH_4Cl solution was added to the solution. The reaction mixture was extracted with hexane and dried over $MgSO_4$. After the solvent was evaporated, purification of the residue by silica gel chromatography (eluent: 7 vol% ethyl acetate in hexane) afforded the title compound as a white solid (786 mg, 1.19 mmol, 54%).

^{1}H NMR (400 MHz, $CDCl_3$, δ): 3.94 (m, 2 H; CH_2), 3.81 (t, $J = 9.6$ Hz, 2 H; CH_2), 3.60 (t, $J = 6.8$ Hz, 2 H; CH_2), 2.19 (t, $J = 7.8$ Hz, 1 H; OH), 1.62–1.55 (m, 2 H; CH_2), 1.37–1.25 (m, 30 H; CH_2), 0.88 (t, $J = 6.8$ Hz, 3 H; CH_3); ^{13}C NMR (100 MHz, $CDCl_3$) δ: 73.40, 32.09, 29.85, 29.73, 29.68, 29.61, 29.52, 29.49, 25.87, 22.85, and 14.28 (only carbons not coupled to fluorine); ^{19}F NMR (376 MHz, $CDCl_3$) δ: −77.49 (2 F; CF_2), −80.37 (2 F; CF_2), −88.60 (4 F; CF_2), −88.80 (4 F; CF_2).

Synthesis of 2,2,4,4,5,5,7,7,8,8,10,10-dodecafluoro-3,6,9,12-tetraoxatriacontan-1-yl methyl carbonate (1a)

Compound **2a** (762 mg, 1.15 mmol) and pyridine (200 μL) in CH_2Cl_2 (15 mL) were stirred at 0 °C. Methyl chloroformate (163 mg, 1.73 mmol) was added dropwise to the solution. The mixture was warmed to room temperature and stirred overnight. Evaporation of the solvent and subsequent purification of the residue by silica gel chromatography (eluent: hexane/CH_2Cl_2 = 2/1) afforded the title compound as a white solid (722 mg, 1.00 mmol, 87%).

^{1}H NMR (400 MHz, $CDCl_3$, δ): 4.52 (t, $J = 9.2$ Hz, 2 H; CH_2), 3.86 (s, 3 H; CH_3), 3.81 (t, $J = 10.0$ Hz, 2 H; CH_2), 3.59 (t, $J = 6.6$ Hz, 2 H; CH_2), 1.62–1.55 (m, 2 H; CH_2), 1.37–1.25 (m, 30 H; CH_2), 0.88 (t, $J = 6.8$ Hz, 3 H; CH_3); ^{13}C NMR (100 MHz, $CDCl_3$) δ: 154.78, 112.02 (td, $J = 281$, 170 Hz), 114.54 (tm, $J = 286$ Hz), 73.26, 69.82 (t, $J = 31$ Hz), 64.74 (t, $J = 34$ Hz), 55.57, 32.19, 29.98, 29.85, 29.80, 29.76, 29.64, 29.60, 26.01, 22.90, and 14.07; ^{19}F NMR (376 MHz, $CDCl_3$) δ: −77.61 (2 F; CF_2), −77.71 (2 F; CF_2), −88.52 (4 F; CF_2), −88.74 (4 F; CF_2); MS (MALDI-TOF) *m/z*: $[M + Na]^+$ calcd for $C_{28}H_{44}F_{12}NaO_7$, 743.28; found, 743.20.

Synthesis of 3,6,9,12-tetraoxatriacontan-1-ol (2b)

A mixture of 1-bromooctadecane (3.90 g, 11.7 mmol), tetraethylene glycol (10.43 g, 53.7 mmol), and NaOH (2.09 g, 52.3 mmol) in water (5 mL) was stirred under reflux for 20 h. The reaction mixture was extracted with hexane, washed with a saturated NH_4Cl solution and water, and dried over $MgSO_4$. After the solvent was evaporated, purification of the residue by silica gel chromatography (eluent: ethyl acetate) yielded the title compound as a white solid (1.58 g, 3.54 mmol, 30%).

^{1}H NMR (400 MHz, $CDCl_3$, δ): 3.75–3.71 (m, 2 H; CH_2), 3.70–3.57 (m, 14 H; CH_2), 3.45 (t, $J = 7.0$ Hz, 2 H; CH_2), 2.73 (t, $J = 6.2$ Hz, 1 H; OH), 1.61–1.54 (m, 2 H; CH_2), 1.35–1.23 (m, 30 H; CH_2), 0.88 (t, $J = 7.0$ Hz, 3 H; CH_3); ^{13}C NMR (100 MHz, $CDCl_3$) δ: 72.67, 71.70, 70.70, 70.44, 70.11, 61,82, 32.03, 29.80, 29.72, 29.67, 29.47, 26.17, 22.79, and 14.22; MS (MALDI-TOF) *m/z*: $[M + Na]^+$ calcd for $C_{26}H_{54}NaO_5$, 469.39; found, 469.38.

Synthesis of 3,6,9,12-tetraoxatriacontan-1-yl methyl carbonate (1b)

Compound **2b** (1.54 g, 3.06 mmol) and pyridine (2.5 mL) in CH_2Cl_2 (30 mL) were stirred at 0 °C. Methyl chloroformate (2.89 g, 30.6 mmol) was added dropwise to the solution. The mixture was warmed to room temperature and stirred overnight. Evaporation of the solvent and subsequent purification of the residue by silica gel chromatography (eluent: ethyl acetate) gave the title compound as a white solid (1.58 g, 1.00 mmol, 91%).

^{1}H NMR (400 MHz, $CDCl_3$, δ): 4.30–4.28 (m, 2 H; CH_2), 3.79 (s, 3 H; CH_3), 3.74–3.71 (m, 2 H; CH_2), 3.68–3.62 (m, 10 H; CH_2), 3.59–3.56 (m, 2 H; CH_2), 3.44 (t, $J = 7.2$ Hz, 2 H; CH_2), 1.61–1.54 (m, 2 H; CH_2), 1.35–1.23 (m, 30 H; CH_2), 0.88 (t, $J = 6.8$ Hz, 3 H; CH_3); ^{13}C NMR (100 MHz, $CDCl_3$) δ: 155.84, 71.65, 70.73, 70.68, 70.14, 69.01, 54.87, 32.01, 29.79, 29.72, 29.59, 29.45, 26.18, 22.78, and 14.21; MS (MALDI-TOF) *m/z*: $[M + Na]^+$ calcd for $C_{28}H_{56}NaO_7$, 527.39; found, 527.68.

Preparation of the complexes of 1a and 1b with LiTFSI

The complexes of **1a** and **1b** with LiTFSI were prepared through slow evaporation of tetrahydrofuran (THF) solutions

Scheme 1 Synthetic scheme for the fluorinated block-structured molecules **1a** and **2a**

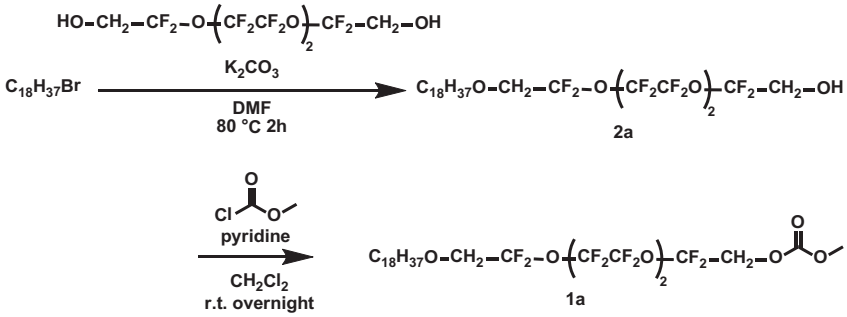

containing the requisite amounts of the compounds and the Li salt followed by drying under reduced pressure at 80 °C.

Measurement of ionic conductivities

The ionic conductivities were measured as a function of the temperature by an alternating current impedance method using a Hioki 3532–80 chemical impedance meter (frequency range: 100 Hz–1 MHz, applied voltage: 0.3 V) equipped with a Linkam LTS 350 hot stage, a Linkam TMS 94 temperature controller, and a Linkam LNP 9412 hot stage cooler (the cooling rate was fixed at 2 K min^{-1}). The ionic conductivities were calculated as the product of the formula $1/R_b$ (Ω^{-1}) (R_b: bulk resistance of the sample) and the cell constant (cm^{-1}) for comb-shaped gold electrodes and were calibrated with the conductivity of a KCl standard solution (HI7033L, 84 μS cm^{-1}) from Hanna Instruments. The impedance data were modeled as a parallel resistor–capacitor circuit in series.

Results and discussion

Material design and synthesis

Oligo (ethylene oxide) monoalkyl ethers have been previously studied for application as nonionic surfactants and detergents [55–63]. The phase behavior and ionic conductivity of lyotropic LC systems of hydrated Li salts and surfactants were also examined [64, 65]. For polymeric systems, poly (methacrylate) comb polymers having alkyl end-capped oligo (ethylene oxide) side chains were developed as nanostructured polymer electrolytes [66]. Perfluorinated ethylene oxide moieties have attracted attention for their fluorophilic self-assembly processes, self-lubricating properties, and good solubility in several polar organic solvents [67]. For example, block-structured ligands consisting of perfluorinated and non-fluorinated oligo (ethylene oxide) segments were used as structure-directing agents for the preparation of size-controlled gold nanoparticles [67–69]. Block copolymers consisting of PFPE and PEO segments were developed, and their electrochemical properties were studied [40, 70]. It should be noted that all the PFPE-based electrolytes previously reported [37, 39–42] form isotropic liquid states except for those electrolytes hybridized with inorganic solids [38] and those cured by thermally or UV activated crosslinking reactions [43]. To the best of our knowledge, the LC behavior and ion-conducting properties of perfluorinated oligo (ethylene oxide) monoalkyl ethers have not yet been studied.

In the present study, we designed and synthesized block-structured molecules with a terminal methyl carbonate **1a** with the expectation of achieving a relatively high ionic conductivity and electrochemical stability for potential application in LIBs (Fig. 2). A dodecyl group was introduced at one end of the perfluorinated oligo (ethylene oxide) moiety. We anticipated that a sufficiently long alkyl chain may introduce LC properties in the block-structured molecules through the packing forces of the chain and the nanosegregation that occurs between fluorous and alkyl moieties. Compared to perfluoroalkyl moieties, perfluorinated oligo (ethylene oxide) compounds are conformationally more flexible owing to the existence of ether oxygens, which may favor ionic conduction in LC structures. The effects of fluoro substituents on the LC properties were also examined for molecule **2a**, which has a hydroxyl group.

Compounds **1a** and **2a** were synthesized according to Scheme 1. Williamson ether synthesis by the reaction of fluorinated tetraethylene glycol with octadecyl bromide in a suspension of potassium carbonate in DMF yielded compound **2a**. Compound **2a** was converted into methyl carbonate-terminated compound **1a** by an esterification reaction with methyl chloroformate in the presence of pyridine as an acid scavenger. Compounds **1b** and **2b** were synthesized by similar procedures.

LC properties of the block-structured molecules

The phase transition properties of block-structured molecules **1a**, **1b**, **2a**, and **2b** were examined by DSC, POM, and XRD. Table 1 compares the phase transition properties of **1a**, **1b**, **2a**, and **2b** on cooling. We denote the unidentified

Table 1 Thermal properties of block-structured molecules 1a, 1b, 2a, and 2b

Sample	Phase transition behavior[a]						
1a	Iso	23 (49.0)	Sm3	5 (1.5)	Sm2	−11 (3.8)	Sm1
1b	Iso	34 (45.8)	Sm3	11 (1.0)	Sm2	−6 (3.4)	Sm1
2a	Iso	32 (43.5)			Sm1	23 (31.7)	Cr
2b	Iso	40 (41.1)	Sm3	12 (0.7)	Sm2	−4 (2.8)	Sm1

[a]Transition temperatures (°C) taken at the onset of the transitions and transition enthalpies (kJ mol^{-1}, given in parentheses) determined by DSC upon 1st cooling at a scanning rate of 10 K min^{-1}. *Cr* crystal, *Iso* isotropic, *Sm1*, *Sm2*, *Sm3* unidentified smectic.

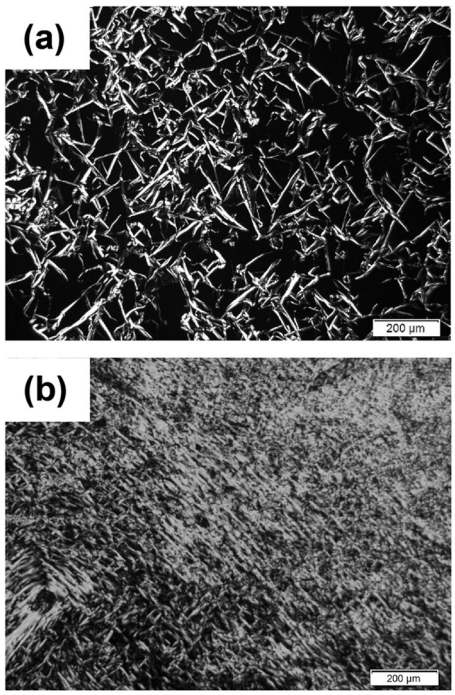

Fig. 3 Polarizing optical micrograph of **1a** at 20 °C in the Sm3 phase **a** before and **b** after applying a mechanical shear force

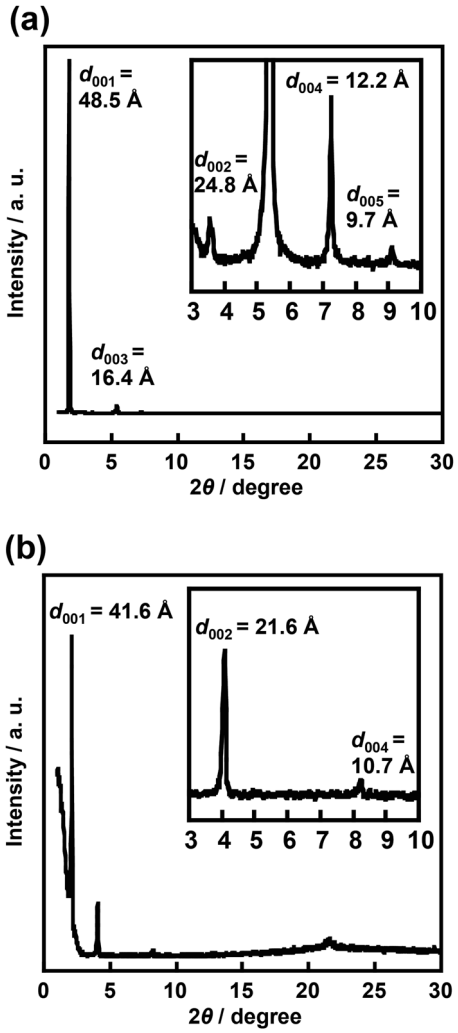

Fig. 4 Wide-angle XRD patterns of **a 1a** and **b 1b** in the Sm3 phase at 20 °C

ordered smectic phases as Sm1, Sm2, and Sm3. Figure 3 shows the POM image of **1a** in the Sm3 phase at 20 °C. A needle-like morphology was observed for **1a** when the sample was placed between glass substrates and cooled from the isotropic phase (Fig. 3a). After applying a mechanical shear force to the sample, its optical texture changed owing to the fluidity of the phase, indicating that the sample formed a soft anisotropic phase (Fig. 3b). The LC structures of **1a** and **1b** in the Sm3 phase at 20 °C were examined by wide-angle XRD (Fig. 4). The XRD pattern of **1a** in the Sm3 phase showed five sharp peaks with *d* values of 48.5, 24.8, 16.4, 12.2, and 9.7 Å (Fig. 4a). The reciprocal *d*-spacing ratio of these values was 1:2:3:4:5, corresponding to the reflections of d_{001}, d_{002}, d_{003}, d_{004}, and d_{005}, respectively. The layer spacing was calculated to be 49 Å from the XRD measurement. The layer spacing was 7 Å larger than the molecular length of **1a** in the fully extended conformation, which was estimated to be 42 Å by molecular mechanics calculations. These results indicate that the Sm3 phase has a highly interdigitated and tilted bilayer structure (Fig. 5). We also estimated the volume ratio of the perfluorinated moiety combined with a terminal methyl carbonate moiety. The combined section occupied nearly half the volume (≃47%) of the entire **1a** molecule, as evaluated from space-filling models. This property could affect the formation of a layered nanosegregated structure by **1a**. In the case of **1b**, the layer spacing of the Sm3 phase was calculated to be 43 Å (Fig. 4b), which was 1 Å larger than the estimated molecular length of **1b** (42 Å). The layer spacing of **1a** in the Sm3 phase was 6 Å larger than that of **1b**, although the molecular length of **1a** was nearly the same as that of **1b**. The DSC thermograms of compounds **1a** and **1b** are shown in Fig. 6. All of the block-structured

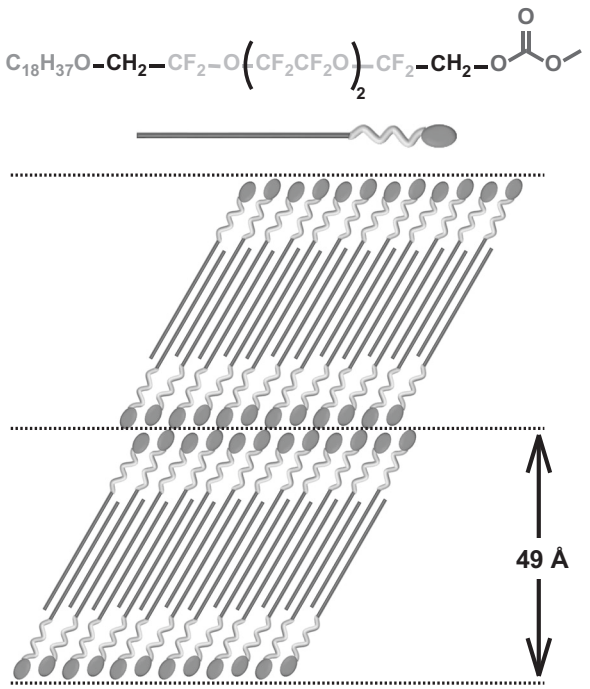

Fig. 5 Proposed assembled structure of **1a** in the Sm3 phase

molecules showed smectic phases near room temperature. For example, compounds **1a** and **1b** exhibited transitions from the isotropic phase to the smectic phase at 23 and 34 °C, respectively, while compounds **2a** and **2b** showed the same transitions at 32 and 40 °C during the cooling process. The enthalpy changes of the transition between the isotropic and the smectic phases on cooling were much larger (41–49 kJ mol^{-1}) than those of the smectic–smectic phase transitions (0.5–3.8 kJ mol^{-1}). These results suggest that the smectic phases have a rather high order for all of these block-structured molecules. From comparison of the phase transition temperatures of **1a** and **1b** with those of **2a** and **2b** (block-structured molecules with different end functional groups), **1a** and **1b** showed lower isotropization temperatures than **2**a and **2b**, respectively. The terminal hydroxyl groups of **2a** and **2b** induced stronger thermal stabilization effects in the smectic phases than the terminal carbonate groups of **1a** and **1b**. The effects of the fluoro substituents were examined through comparison of the transition temperatures. It is noteworthy that the isotropization temperatures of fluorinated compounds **1a** and **2a** were lower than those of the analogous non-fluorinated compounds **1b** and **2b**, respectively. This observation differs from the general trend, [44–47, 54] in which perfluoro substituents on the terminal alkyl chains of LC molecules promote stabilized nanosegregation, thus leading to the formation of thermally more stable LC structures. The fluoro substituents in the oligo (ethylene oxide) moieties may destabilize the packing structures of the highly ordered smectic phases, which is most likely due to the steric hindrance of the fluorine atoms. The effects of the fluoro

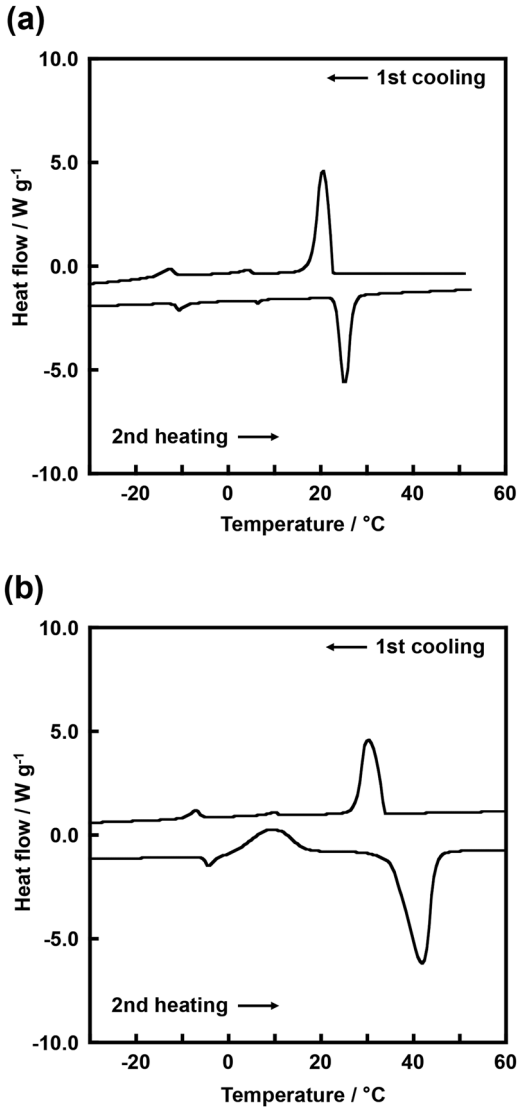

Fig. 6 DSC thermograms of block-structured molecules **1a** (**a**) and **1b** (**b**) obtained at a scanning rate of 10 K min^{-1}

substituents led to lower isotropization temperatures for the fluorinated block-structured molecules (**1a** and **2a**) than for the non-fluorinated molecules (**1b** and **2b**). This explanation is supported by the physical properties of PFPEs recently determined from molecular simulations combined with experiments in a report by Black et al. [71]; this study suggests that PFPEs have a reduced cohesive energy than PEOs due to their lower overall polarity and weaker intermolecular interactions.

LC behavior and ionic conductivities of complexes formed from the block-structured molecules and LiTFSI

The ion-conducting properties of the complexes formed from **1a** and **1b** with LiTFSI as LC electrolytes were

examined. The complexes were prepared by slow evaporation of THF solutions containing the requisite amount of the compounds and the Li salt. Compound **1a** formed homogeneous mixtures with up to 60 mol% LiTFSI. The complexes formed from **1a** and **1b** with LiTFSI also exhibited smectic phases. The complex of **1a** with 60 mol% LiTFSI showed a transition from the isotropic phase to the smectic phase at 34 °C, which was 11 °C higher than the transition of **1a** alone. In contrast, the complex of **1b** with 60 mol% LiTFSI exhibited an isotropization transition at 33 °C, which was 1 °C lower than that of **1b** alone. The different trends in the transition temperatures of **1a** and **1b** when complexed with LiTFSI can possibly be attributed to the different coordination states of **1a** and **1b** with Li cations. In the case of **1a**, the terminal carbonate moieties coordinate to Li cations, resulting in strong intermolecular interactions through ion–dipole interactions of Li cations and the carbonate moieties. The Li cations and TFSI anions can be located at the extremities of **1a**. These effects lead to a more stabilized nanostructure and a higher isotropization temperature for the complex of **1a** with LiTFSI than for **1a** alone, as is often observed in other carbonate-based LC electrolyte systems [19, 22, 30]. On the other hand, in the complex of **1b** with LiTFSI, in addition to the carbonate moieties, the oligoether moieties can also coordinate to Li cations. Although the addition of LiTFSI could promote nanosegregation of the molecules, the incorporation of Li cations and TFSI anions within the smectic layers of the oligo (ethylene oxide) moieties may destabilize the relatively highly ordered packing structure of **1b** due to the steric bulk of the ion pairs.

The ionic conductivities of these complexes were measured as a function of temperature by an alternating current impedance method. The measurement was conducted using comb-shaped gold electrodes deposited on a glass substrate during the cooling process. Figure 7 presents the ionic conductivities of **1a** and **1b** complexed with 60 mol% LiTFSI. For comparison, the ionic conductivities of a low-molecular-weight liquid PFPE-based electrolyte (PFPE-DMC in Fig. 1) [37] and a poly(ethylene glycol) electrolyte [39] are also given in Fig. 7. The complex of **1a** exhibited ionic conductivities on the order of 10^{-6} and 10^{-5} S cm^{-1} in the ordered smectic phase at approximately 30 °C and in the isotropic temperature range of 40–100 °C, respectively. For example, the complex of **1a** showed conductivities of 3.6×10^{-6} and 1.7×10^{-5} S cm^{-1} in the smectic phase at 30 °C and in the isotropic phase at 60 °C, respectively. These values were similar to those of the PFPE-based electrolyte. [37] The ionic conductivities of the complex of **1b** were close to those of the poly (ethylene glycol) electrolyte [39]. The values were approximately one order of magnitude higher than those of the complex of **1a**. The lower conductivities of **1a** compared to those of **1b** can be explained

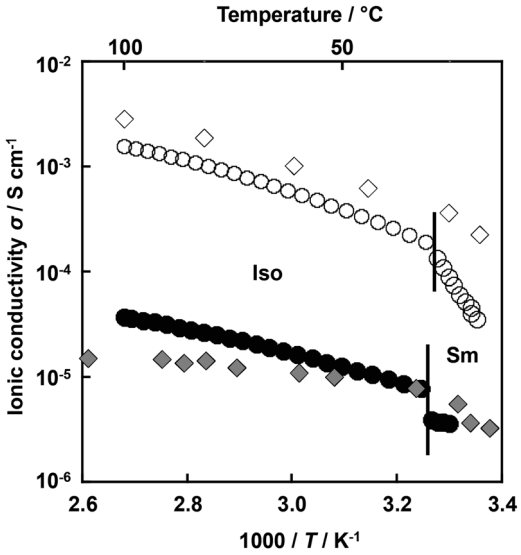

Fig. 7 Ionic conductivities of block-structured molecules **1a** (closed circle: ●) and **1b** (open circle: ○) complexed with 60 mol% LiTFSI during cooling. For comparison, the ionic conductivities of the methyl carbonate-terminated PFPE electrolyte [37] (PFPE-DMC in Fig. 1) (gray diamond: ♦) and the poly(ethylene glycol) electrolyte [39] (open diamond: ◇) are also given

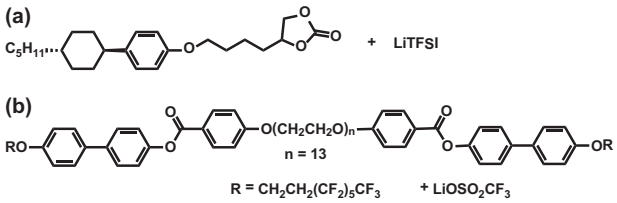

Fig. 8 Molecular structures of the cyclic carbonate-based LC electrolyte [30] (**a**) and the LC compound having perfluoroalkyl-terminated mesogens at both ends of a PEO chain complexed with lithium triflate [54] (**b**)

as follows: perfluorinated oligo (ethylene oxide) moieties do not coordinate to Li cations. The dissociation and transport of Li ions are affected by the terminal methyl carbonate moiety present in **1a**. On the other hand, the oligo (ethylene oxide) moiety of **1b** can contribute to the dissociation and transport of Li cations in addition to the contribution of the carbonate moiety. These effects led to higher ionic conductivities for **1b** than for **1a**. A sharp decrease in the ionic conductivity on cooling was observed at the phase transitions from the isotropic phase to the smectic phase that occurred at 34 and 33 °C for the complexes of **1a** and **1b**, respectively. This behavior is due to the formation of unaligned polydomains and the higher viscosity of the ordered smectic phase, in which the mobility of the molecules and ions is lower than that in the isotropic phase.

We compared the ionic conductivities of the complexes of **1a** and **1b** with those of other LC electrolytes (Figs. 8

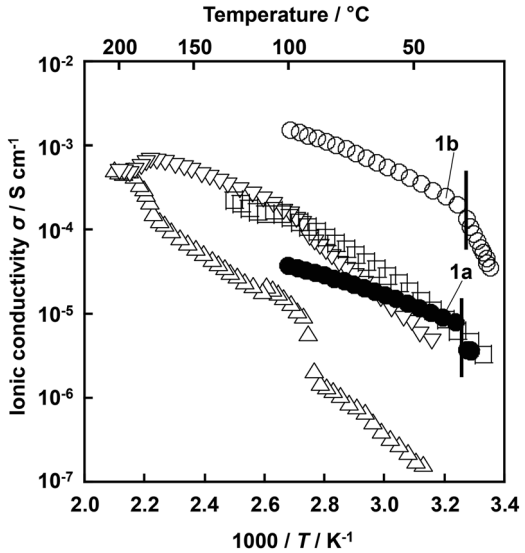

Fig. 9 Ionic conductivities of the LC electrolytes of **1a** (closed circle: ●) and **1b** (open circle: ○) complexed with 60 mol% LiTFSI, the cyclic carbonate-based LC compound complexed with 10 mol% LiTFSI [30] (Fig. 8a) (square: □), and the LC compound having a perfluoroalkyl-terminated mesogen at both ends of a PEO chain complexed with lithium triflate ($Li^+/CH_2CH_2O = 0.05$) [54] (Fig. 8b) (conductivities parallel to the smectic layers of the aligned monodomain sample (inverted triangle: ▽) and the unaligned polydomain sample (triangle: △))

and 9). Figure 8 shows the molecular structures of the components of a cyclic carbonate-based LC electrolyte complexed with LiTFSI [30] (Fig. 8a) and a PEO-based LC electrolyte bearing perfluoroalkyl groups complexed with lithium triflate [54] (Fig. 8b). These LC electrolytes aligned homeotropically when the samples were sandwiched between glass substrates. The aligned LC electrolytes showed effective ion conduction in the direction parallel to the smectic layers (squares and inverted triangles plotted in Fig. 9). On the other hand, both the complexes of **1a** and **1b** formed unaligned polydomains in the smectic phases, resulting in a decrease in the conductivity at the transition from the isotropic phase to the smectic phase. However, it should be noted that the ionic conductivities of the complex of **1a** in the temperature range of the smectic phase (~30 °C) are comparable to those of the carbonate-based LC electrolyte and the PEO-based LC electrolyte in the aligned monodomain state.

Conclusions

Perfluorinated oligo (ethylene oxide) monoalkyl ethers containing a terminal methyl carbonate or a hydroxyl moiety were developed for potential application as quasi-solid-state electrolytes for LIBs. Both the fluorinated and non-fluorinated molecules formed highly ordered smectic phases near room temperature. The introduction of fluoro substituents in the oligo (ethylene oxide) moieties lowered the isotropization temperatures of the block-structured molecules. The complexes formed between the fluorinated block-structured molecule and the Li salt showed ionic conductivities on the order of 10^{-6} S cm^{-1} and 10^{-5} S cm^{-1} in the smectic and the isotropic phases, respectively. The ionic conductivities of the complexes formed from the fluorinated block-structured molecule were lower than those formed from the non-fluorinated molecule.

Nanostructured molecular assemblies containing perfluorinated moieties have potential for application as transport materials.

Acknowledgements TO is grateful for the support from the Japan Society for the Promotion of Science through the Program for Leading Graduate Schools (MERIT).

Compliance with ethical standards

Conflict of interest The authors declare that they have no conflict of interest.

References

1. Kato T, Yoshio M, Ichikawa T, Soberats B, Ohno H, Funahashi M. Transport of ions and electrons in nanostructured liquid crystals. Nat Rev Mater. 2017;2:17001.
2. Kato T. From nanostructured liquid crystals to polymer-based electrolytes. Angew Chem Int Ed. 2010;49:7847–7848.
3. Yoshio, M & Kato, T Handbook of Liquid Crystals 8. In Goodby J, Collings PJ, Kato T, Tschierske C, Gleeson H & Raynes P, editors. Ch. 23 (Wiley-VCH Verlag KGaA, Weinheim, 2014).
4. Zheng Y, Lui J, Ungar G, Wright PV. Solvent-free low-dimensional polymer electrolytes for lithium-polymer batteries. Chem Rec. 2004;4:176–191.
5. Goossens K, Lava K, Bielawski CW, Binnemans K. Ionic liquid crystals: versatile materials. Chem Rev. 2016;116:4643–4807.
6. Cho B-K. Nanostructured organic electrolytes. RSC Adv. 2014;4:395–405.
7. Cho B-K. Spontaneous bulk organization of molecular assemblers based on aliphatic polyether and/or poly(benzyl ether) dendrons. Polym J. 2012;44:475–489.
8. Ichikawa T. Zwitterions as building blocks for functional liquid crystals and block copolymers. Polym J. 2017;49:413–421.
9. Kato T. Self-assembly of phase-segregated liquid crystal structures. Science. 2002;295:2414–2418.
10. Kumar M, Kumar S. Liquid crystals in photovoltaics: a new generation of organic photovoltaics. Polym J. 2017;49:85–111.
11. Xiao Y, Zeng D, Mazur LM, Castiglione A, Lacaze E, Heinrich B, Donnio B, Kreher D, Attias AJ, Ribierre JC, Mathevet F. A new class of nanostructured supramolecular organic semiconductors based on intertwined multi-lamellar co-assemblies in π-conjugated liquid-crystalline side-chain polymers. Polym J. 2017;49:31–39.
12. Funahashi M. Integration of electro-active π-conjugated units in nanosegregated liquid-crystalline phases. Polym J. 2017;49:75–83.

13. Iino H, Hanna JI. Liquid crystalline organic semiconductors for organic transistor applications. Polym J. 2017;49:23–30.
14. Broer DJ, Bastiaansen CMW, Debije MG, Schenning APHJ. Functional organic materials based on polymerized liquid-crystal monomers: Supramolecular hydrogen-bonded systems. Angew Chem Int Ed. 2012;51:7102–7109.
15. Wiesenauer BR, Gin DL. Nanoporous polymer materials based on self-organized, bicontinuous cubic lyotropic liquid crystal assemblies and their applications. Polym J. 2012;44:461–468.
16. Kato T, Uchida J, Ichikawa T, Soberats B. Functional liquid-crystalline polymers and supramolecular liquid crystals. Polym J. 2018;50:149–166.
17. Marets N, Kuo D, Torrey JR, Sakamoto T, Henmi M, Katayama H, Kato T. Highly efficient virus rejection with self-organized membranes based on a crosslinked bicontinuous cubic liquid crystal. Adv Healthc Mater. 2017;6:1700252.
18. Sakamoto T, Ogawa T, Nada H, Nakatsuji K, Mitani M, Soberats B, Kawata K, Yoshio M, Tomioka H, Sasaki T, Kimura M, Henmi M, Kato T. Development of nanostructured water treatment membranes based on thermotropic liquid crystals: molecular design of sub-nanoporous materials. Adv Sci. 2017;5:1700405.
19. Shimura H, Yoshio M, Hamasaki A, Mukai T, Ohno H, Kato T. Electric-field-responsive lithium-ion conductors of propylenecarbonate-based columnar liquid crystals. Adv Mater. 2009;21:1591–1594.
20. Yoshio M, Mukai T, Ohno H, Kato T. One-dimensional ion transport in self-organized columnar ionic liquids. J Am Chem Soc. 2004;126:994–995.
21. Ohtake T, Ito K, Nishina N, Kihara H, Ohno H, Kato T. Liquid-crystalline complexes of a lithium salt with twin oligomers containing oxyethylene spacers. an approach to anisotropic ion conduction. Polym J. 1999;31:1155–1158.
22. Eisele A, Kyriakos K, Bhandary R, Schönhoff M, Papadakis CM, Rieger B. Structure and ionic conductivity of liquid crystals having propylene carbonate units. J Mater Chem A. 2015;3:2942–2953.
23. Lee JH, Han KS, Lee JS, Lee AS, Park SK, Hong SY, Lee JC, Mueller KT, Hong SM, Koo CM. Facilitated ion transport in smectic ordered ionic liquid crystals. Adv Mater. 2016;28:9301–9307.
24. Rondla R, Lin JCY, Yang CT, Lin IJB. Strong tendency of homeotropic alignment and anisotropic lithium ion conductivity of sulfonate functionalized zwitterionic imidazolium ionic liquid crystals. Langmuir. 2013;29:11779–11785.
25. Ichikawa T, Yoshio M, Hamasaki A, Taguchi S, Liu F, Zeng X, Ungar G, Ohno H, Kato T. Induction of thermotropic bicontinuous cubic phases in liquid-crystalline ammonium and phosphonium salts. J Am Chem Soc. 2012;134:2634–2643.
26. Soberats B, Yoshio M, Ichikawa T, Ohno H, Kato T. Zwitterionic liquid crystals as 1D and 3D lithium ion transport media. J Mater Chem A. 2015;3:11232–11238.
27. Kobayashi T, Ichikawa T, Kato T, Ohno H. Development of glassy bicontinuous cubic liquid crystals for solid proton-conductive materials. Adv Mater. 2017;29:1604429.
28. Kerr RL, Miller Sa, Shoemaker RK, Elliott BJ, Gin DL. New type of Li ion conductor with 3D interconnected nanopores via polymerization of a liquid organic electrolyte-filled lyotropic liquid-crystal assembly. J Am Chem Soc. 2009;131:15972–15973.
29. Kerr RL, Edwards JP, Jones SC, Elliott BJ, Gin DL. Effect of varying the composition and nanostructure of organic carbonate-containing lyotropic liquid crystal polymer electrolytes on their ionic conductivity. Polym J. 2016;48:635–643.
30. Sakuda J, Hosono E, Yoshio M, Ichikawa T, Matsumoto T, Ohno H, Zhou H, Kato T. Liquid-crystalline electrolytes for lithium-ion batteries: ordered assemblies of a mesogen-containing carbonate and a lithium salt. Adv Funct Mater. 2015;25:1206–1212.
31. Onuma T, Hosono E, Takenouchi M, Sakuda J, Kajiyama S, Yoshio M, Kato T. Noncovalent approach to liquid-crystalline ion conductors: high-rate performances and room-temperature operation for Li-ion batteries. ACS Omega. 2018;3:159–166.
32. Berthier C, Gorecki W, Minier M, Armand MB, Chabagno JM, Rigaud P. Microscopic investigation of ionic conductivity in alkali metal salts-poly(ethylene oxide) adducts. Solid State Ion. 1983;11:91–95.
33. Nishimoto A, Watanabe M, Ikeda Y, Kohjiya S. High ionic conductivity of new polymer electrolytes based on high molecular weight polyether comb polymers. Electrochim Acta. 1998;43:1177–1184.
34. Borodin O, Smith GD. Mechanism of ion transport in amorphous poly(ethylene oxide)/LiTFSI from molecular dynamics simulations. Macromolecules. 2006;39:1620–1629.
35. Plenio H. The coordination chemistry of the CF unit in fluorocarbons. Chem Rev. 1997;97:3363–3384.
36. Lin TY, Lin WH, Clark WD, Larson SB, Simonsen SH, Lynch VM, Brodbelt JS, Maleknia SD, Liou CC, Lagow RJ. Synthesis and chemistry of perfluoro macrocycles. J Am Chem Soc. 1994;116:5172–5179.
37. Wong DHC, Thelen JL, Fu Y, Devaux D, Pandya AA, Battaglia VS, Balsara NP, Desimone JM. Nonflammable perfluoropolyether-based electrolytes for lithium batteries. Proc Natl Acad Sci USA. 2014;111:3327–3331.
38. Villaluenga I, Wujcik KH, Tong W, Devaux D, Wong DHC, DeSimone JM, Balsara NP. Compliant glass–polymer hybrid single ion-conducting electrolytes for lithium batteries. Proc Natl Acad Sci USA. 2015;113:52–57.
39. Wong DHC, Vitale A, Devaux D, Taylor A, Pandya AA, Hallinan DT, Thelen JL, Mecham SJ, Lux SF, Lapides AM, Resnick PR, Meyer TJ, Kostecki RM, Balsara NP, Desimone JM. Phase behavior and electrochemical characterization of blends of perfluoropolyether, poly (ethylene glycol), and a lithium salt. Chem Mater. 2015;27:597–603.
40. Chintapalli M, Timachova K, Olson KR, Mecham SJ, Devaux D, Desimone JM, Balsara NP. Relationship between conductivity, ion diffusion, and transference number in perfluoropolyether electrolytes. Macromolecules. 2016;49:3508–3515.
41. Olson KR, Wong DHC, Chintapalli M, Timachova K, Januszie-wicz R, Daniel WFM, Mecham S, Sheiko S, Balsara NP, DeSimone JM. Liquid perfluoropolyether electrolytes with enhanced ionic conductivity for lithium battery applications. Polym (Guildf). 2016;100:126–133.
42. Timachova K, Chintapalli M, Olson KR, Mecham SJ, DeSimone JM, Balsara NP. Mechanism of ion transport in perfluoropolyether electrolytes with a lithium salt. Soft Matter. 2017;13:5389–5396.
43. Devaux D, Villaluenga I, Bhatt M, Shah D, Chen XC, Thelen JL, DeSimone JM, Balsara NP. Crosslinked perfluoropolyether solid electrolytes for lithium ion transport. Solid State Ion. 2017;310:71–80.
44. Guittard F, Taffin de Givenchy E, Geribaldi S, Cambon A. Highly fluorinated thermotropic liquid crystals: an update. J Fluor Chem. 1999;100:85–96.
45. Hird M. Fluorinated liquid crystals—properties and applications. Chem Soc Rev. 2007;36:2070–2095.
46. Tschierske C. Fluorinated liquid crystals: design of soft nanostructures and increased complexity of self-assembly by perfluorinated segments. Top Curr Chem. 2012;318:1–108.
47. Tshierske,C Handbook of Liquid Crystals 5 In: Goodby J, Collings PJ, Kato T, Tschierske C, Gleeson H & Raynes P, editors. Ch. 2 (Wiley-VCH Verlag KGaA, Weinheim, 2014).
48. Rabolt JF, Russell TP, Twieg RJ. Structural studies of semi-fluorinated *n*-alkanes. 1. Synthesis and characterization of $F(CF_2)_n(CH_2)_mH$ in the solid state. Macromolecules. 1984;17:2786–2794.

49. Mahler W, Guillon D, Skoulios A. Smectic liquid crystal from (perfluorodecyl)decane. Mol Cryst Liq Cryst Lett. 1985;2: 111–119.
50. Viney C, Twieg RJ, Russell TP, Depero LE. The structural basis of transitions between highly ordered smectic phases in semi-fluorinated alkanes. Liq Cryst. 1989;5:1783–1788.
51. Viney C, Russell TP, Depero LE, Twieg RJ. Transitions to liquid crystalline phases in a semifluorinated alkane. Mol Cryst Liq Cryst Inc Nonlinear Opt. 1989;168:63–82.
52. Höpken J, Möller M. On the morphology of (perfluoroalkyl) alkanes. Macromolecules. 1992;25:2482–2489.
53. Fujiwara M, Satoh K, Kondo S, Ujiie S. Liquid crystalline properties and molecular packing of semifluorinated *n*-alkanes F $(CF_2)_{10}(CH_2)_mH$. Macromolecules. 2006;39:5836–5842.
54. Hoshino K, Kanie K, Ohtake T, Mukai T, Yoshizawa M, Ujiie S, Ohno H, Kato T. Ion-conductive liquid crystals: formation of stable smectic semi-bilayers by the introduction of perfluoroalkyl moieties. Macromol Chem Phys. 2002;203:1547–1555.
55. Wrigley AN, Stirton AJ, Howard E. Higher alkyl monoethers of mono- to tetraethylene glycol. J Org Chem. 1960;25:439–444.
56. Dorset DL. Molecular conformation and crystal packing of *n*-alkyl oligo (ethylene oxides). J Colloid Interface Sci. 1983;96:172–181.
57. Shinoda K, Fukuda M, Carlsson A. Characteristic solution properties of mono-, di-, and triglyceryl alkyl ethers: lipophobicity of hydrophilic groups. Langmuir. 1990;6:334–337.
58. Craven JR, Hao Z, Booth C. Crystallinity of uniform oligo(oxyethylene) mono-n-alkyl ethers studied by X-ray diffraction and differential scanning calorimetry. J Chem Soc Faraday Trans. 1991;87:1183–1186.
59. Matsuura H, Fukuhara K, Masatoki S, Sakakibara M. Molecular conformation of nonionic surfactants in the solid state. A Raman spectroscopic study of a homologous series of α-*n*-alkyl-ω-hydroxyoligo(oxyethylenes). J Am Chem Soc. 1991;113:1193–1202.
60. Kato T, Taguchi N, Terao T, Seimiya T. Structure of networks formed in concentrated solutions of nonionic surfactant studied by the pulsed-gradient spin-echo method. Langmuir. 1995;11:4661–4664.
61. Shinoda K, Carlsson A, Lindman B. On the importance of hydroxyl groups in the polar head-group of nonionic surfactants and membrane lipids. Adv Colloid Interface Sci. 1996;64:253–271.
62. Celik Ö, Dag Ö. A new lyotropic liquid crystalline system: oligo (ethylene oxide) surfactants with $[M(H_2O)_n]X_m$ transition metal complexes. Angew Chem Int Ed. 2001;40:3799–3803.
63. Zinn T, Willner L, Lund R, Pipich V, Appavou M-S, Richter D. Surfactant or block copolymer micelles? Structural properties of a series of well-defined *n*-alkyl–PEO micelles in water studied by SANS. Soft Matter. 2014;10:5212–5220.
64. Albayrak C, Cihaner A, Dag Ö. A new, highly conductive, lithium salt/nonionic surfactant, lyotropic liquid-crystalline mesophase and its application. Chem Eur J. 2012;18:4190–4194.
65. Balci FM, Balci S, Kocabas C, Dag Ö. Lyotropic liquid-crystalline mesophase of lithium triflate-nonionic surfactant as gel electrolyte for graphene optical modulator. J Phys Chem C. 2017;121:11194–11200.
66. Liu G, Reinhout M, Mainguy B, Baker GL. Synthesis, structure, and ionic conductivity of self-assembled amphiphilic poly (methacrylate) comb polymers. Macromolecules. 2006;39:4726–4734.
67. Nishio T, Niikura K, Matsuo Y, Ijiro K. Self-lubricating nanoparticles: self-organization into 3D-superlattices during a fast drying process. Chem Commun. 2010;46:8977–8979.
68. Niikura K, Iyo N, Higuchi T, Nishio T, Jinnai H, Fujitani N, Ijiro K. Gold nanoparticles coated with semi-fluorinated oligo (ethylene glycol) produce sub-100 nm nanoparticle vesicles without templates. J Am Chem Soc. 2012;134:7632–7635.
69. Wei J, Niikura K, Higuchi T, Kimura T, Mitomo H, Jinnai H, Joti Y, Bessho Y, Nishino Y, Matsuo Y, Ijiro K. Yolk/shell assembly of gold nanoparticles by size segregation in solution. J Am Chem Soc. 2016;138:3274–3277.
70. Chintapalli M, Timachova K, Olson KR, Banaszak M, Thelen JL, Mecham SJ, DeSimone JM, Balsara NP, Lux SF, Lapides AM, Resnick PR, Meyer TJ, Kostecki RM, Desimone JM. Incipient microphase separation in short chain perfluoropolyether-block-poly(ethylene oxide) copolymers. Soft Matter. 2017;13:4047–4056.
71. Black JE, Silva GMC, Klein C, Iacovella CR, Morgado P, Martins LFG, Filipe EJM, McCabe C. Perfluoropolyethers: development of an all-atom force field for molecular simulations and validation with new experimental vapor pressures and liquid densities. J Phys Chem B. 2017;121:6588–6600.